Experimental Confirmation of an HF Channel Model

CLARK C. WATTERSON, JOHN R. JUROSHEK, AND WILLIAM D. BENSEMA, MEMBER, IEEE

Abstract—Specially designed HF ionospheric propagation measurements were made and analyzed to confirm the validity and bandwidth limitations of a proposed stationary HF ionospheric channel model. In the model, the input (transmitted) signal feeds an ideal delay line and is delivered at several taps with adjustable delays, one for each resolvable ionospheric modal component. Each delayed signal is modulated in amplitude and phase by a baseband tap-gain function, and the delayed and modulated signals are summed (with additive noise) to form the output (received) signal. Statistical specifications for the tap-gain functions involved three hypotheses: 1) that each tap-gain function is a complex-Gaussian process that produces Rayleigh fading, 2) that the tap-gain functions are independent, and 3) that each tap-gain function has a spectrum that in general is the sum of two Gaussian functions of frequency, one for each magnetoionic component. Statistical tests were performed on daytime and nighttime measurements confirming the validity of the three hypotheses, and thereby the validity of the model. For practical applications, the model can be considered valid over a bandwidth equal to about one fourth of the reciprocal of the effective (weighted) time spreads on the ionospheric modal components. The model should be useful both in theoretical analyses of communication system performance and for channel simulator designs.

INTRODUCTION

TWO METHODS are commonly used to evaluate the performance of HF radio communication systems: theoretical analyses and experimental measurements. Both are desirable, and each has its advantages and limitations.

In theoretical analyses of system performance, a variety of HF channel models have been used. Usually the model consists of a single path with either no fading or slow (nondistorting) Rayleigh fading, although increasing attention is being given to more realistic channel models that incorporate time-spread (multipath) distortion and/or frequency-spread (fading) distortion [1]–[8].

Experimental measurements of system performance have usually been made over actual ionospheric links, but they are usually difficult both to obtain and to apply. Most of the difficulties can be avoided when experimental measurements are made with a stationary channel simulator in the laboratory. Consequently, there has been a rapidly growing interest in the development of HF channel simu-

lators [9]–[21]. While channel simulator measurements can never completely replace on-the-air measurements, they have a number of substantial advantages.

System performance evaluations obtained from theoretical analyses and experimental measurements on a channel simulator have one thing in common: both are based on HF channel models that can be described mathematically. The number and variety of the models that have been used in theoretical and experimental work is surprising (e.g., the 13 channel simulators referenced previously are based on 11 different channel models). While an unproven channel model can provide very useful information, results must be used with caution; they may not be typical of the HF medium. Preferably, both for theoretical analyses and as the basis for simulator designs, one would like a mathematically tractable channel model that is known to be a valid representation of the HF medium for as large a percentage of typical HF links as practical. But some of the detailed characteristics of the ionosphere needed to specify such a channel model have not been available. Therefore, we undertook a program in 1965 to develop specialized propagation measuring equipment, to obtain measurements of some typical ionospheric channels, and to analyze the measurements to determine the validity and bandwidth limitations of a proposed channel model (exclusive of additive noise). The model we proposed, the measurement and analysis methods we used, and the results we obtained are the subject of this paper.

CHANNEL MODEL

HF ionospheric channels are nonstationary in both frequency and time, but if consideration is restricted to band-limited channels (say, 10 kHz) and sufficiently short times (say, 10 minutes), most channels are nearly stationary and can be adequately represented by a stationary model. The ionosphere exhibits another fortunate characteristic: in a substantial percentage of the channels, propagation is over a limited number of relatively discrete modes. These characteristics allowed us to select the stationary channel model illustrated in Fig. 1. The input (transmitted) signal feeds an ideal delay line and appears at a limited number of taps with adjustable delays. The signal at each tap is modulated in amplitude and phase by a suitable baseband tap-gain function $G_i(t)$, and the several delayed and modulated signals are summed to form the output (received) signal. One tap or path is used for each modal component that is resolvable in time. While each mode in general contains four components
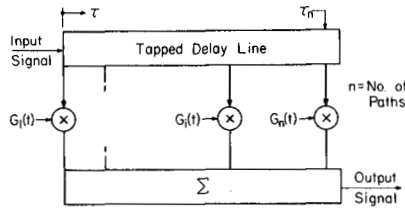
Fig. 1. Channel model.

(the ordinary and extraordinary magnetoionic components of both the low and high rays), all four when present are not necessarily resolvable. Any pair of components is resolvable only when their differential propagation time is greater than about one fourth of the reciprocal of the bandwidth of interest. Consequently, for bandwidths as large as 10 kHz, the two magnetoionic components in the low ray are usually not resolvable, and a single tap will serve both components. When present, the high ray is usually sufficiently delayed from the low ray to be resolvable and therefore require at least one additional tap (unless the bandwidth is very small), and often the two magnetoionic components in the high ray are resolvable, requiring a pair of taps.

The channel model of Fig. 1 is a general model until the characteristics of the tap-gain functions are specified. An infinite variety of specific models is possible. All but one of the previously referenced channel simulators [15] are stationary and based on this same general model, but with two exceptions, all in general use different specifications for $\{G_i(t)\}$. Before describing our own specific model, several mathematical descriptions of the general model will be defined.

The time-varying frequency response of the model can be seen to be

$$H(f,t) = \sum_{i=1}^{n} \exp\left(-j2\pi\tau_i f\right) G_i(t) \qquad (1)$$

where i is an integer that numbers the tap or path, τ_i is the time delay on the ith path, and n is the total number of paths.

Since $\{G_i(t)\}$ and $H(f,t)$ are random processes, they must be described in statistical terms. One such description for each tap-gain function is the tap-gain correlation function

$$C_i(\Delta t) = E[G_i^*(t)G_i(t + \Delta t)] \qquad (2)$$

where E means the expected or mean value and the asterisk denotes a complex conjugate. Then the tap-gain spectrum is defined as the Fourier transform on Δt of the tap-gain correlation function

$$v_i(\nu) = F[C_i(\Delta t)] \qquad (3)$$

where F indicates the Fourier transform.

The channel can also be described in a similar way [22]–[24]. The channel correlation function is

$$R(\Delta f,\Delta t) = E[H^*(f,t)H(f + \Delta f, t + \Delta t)] \qquad (4)$$

which, for the general model of Fig. 1, becomes the following:

$$R(\Delta f,\Delta t) = \sum_{i=1}^{n} \exp\left(-j2\pi\tau_i\Delta f\right) C_i(\Delta t) \qquad (5)$$

provided the tap-gain functions are uncorrelated. The channel scatter function is defined as the double Fourier transform on Δf and Δt of $R(\Delta f,\Delta t)$, which, for the general model of Fig. 1, is

$$s(\tau,\nu) = \sum_{i=1}^{n} \delta(\tau - \tau_i)v_i(\nu) \qquad (6)$$

where $\delta(\tau)$ is the Dirac delta function.

Since $G_i(t)$ and $H(f,t)$ are dimensionless, $C_i(\Delta t)$ and $R(\Delta f,\Delta t)$ are also dimensionless, but with zero arguments they can be viewed as power ratios (or attenuations). $C_i(0)$ is the ratio of the output power delivered by the ith path to the channel input power, and $R(0,0)$ is the ratio of the channel output power to the channel input power. Then $v_i(\nu)$ and $s(\tau,\nu)$ are power-ratio density functions; $v_i(\nu)$ is the ratio of the output power per unit frequency offset over the ith path to the channel input power, while $s(\tau,\nu)$ is the ratio of the channel output power per unit frequency offset per unit time delay to the channel input power.

While the choice of the general model of Fig. 1 was relatively easy, the choice of a specific model was less so. Measurements by Shaver *et al.* [25] indicated that most channels have zero-mean complex-Gaussian statistics, but it is possible that near-Gaussian channel characteristics might be produced by several modes of comparable strength, each of which does not have Gaussian statistics. Measurements on individual modal components by Balser and Smith [26], however, showed the majority produced Rayleigh fading (implying zero-mean complex-Gaussian characteristics), and this is supported by measurements of Boys [27]. We therefore decided that each tap-gain function in the specific channel model should be an independent zero-mean complex-Gaussian function with Rayleigh amplitude and uniform phase density functions.

In addition, we needed to specify the tap-gain spectrums. Since data were not available on the shapes of the spectrums, we arbitrarily chose a Gaussian shape for each magnetoionic component. The subsequent measurements and analyses showed this choice was a good one. Even when a single tap or path can be used for the two magnetoionic components, such as for the low ray, two Gaussian spectrum components were still used, because measurements by Davies [28] and Shepherd and Lomax [29] had shown that the two components can be resolved in frequency. This two-component tap-gain spectrum is illustrated in Fig. 2. Six parameters define it: the power ratios of the two magnetoionic components $C_{sia}(0)$ and $C_{sib}(0)$; the frequency shifts ν_{sia} and ν_{sib}; and the frequency spreads $2\sigma_{sia}$ and $2\sigma_{sib}$. (The a and b subscripts identify the magnetoionic components, and the s subscript designates quantities in our specific channel model.) When the
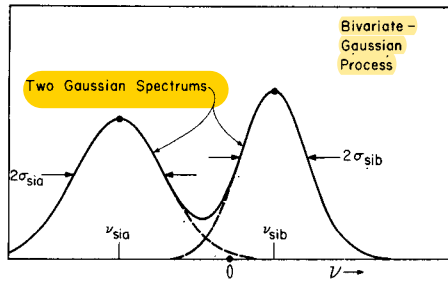
Fig. 2. Tap-gain spectrum in channel model.

frequency shifts and frequency spreads of the two magnetoionic components are approximately equal and they appear as one, only a single Gaussian function is required in the tap-gain spectrum. When separate taps are used for the two components in the high ray, each tap-gain spectrum of course is a single Gaussian function.

To be explicit, the specific channel model that we selected had independent tap-gain functions, each of which is defined in general by

$$G_{si}(t) = G_{sia}(t) \exp\left(j2\pi\nu_{sia}t\right) + G_{sib}(t) \exp\left(j2\pi\nu_{sib}t\right). \tag{7}$$

$G_{sia}(t)$ and $G_{sib}(t)$ are two independent complex (bivariate)-Gaussian stationary ergodic random processes, each with zero-mean values and independent quadrature components with equal rms values and identical spectrums. Specifically, if $G_{sia}(t)$ is defined in terms of its real and imaginary components by

$$G_{sia}(t) = g_{sia}(t) + j\boldsymbol{g}_{sia}(t) \tag{8}$$

then $g_{sia}(t)$ and $\boldsymbol{g}_{sia}(t)$ are independent real Gaussian processes with the following single-time joint density function:

$$p(g_{sia}, \boldsymbol{g}_{sia}) = \frac{1}{\pi C_{sia}(0)} \exp\left[-\frac{g_{sia}^2 + \boldsymbol{g}_{sia}^2}{C_{sia}(0)}\right] \tag{9}$$

where $C_{sia}(0)$ is the autocorrelation of (8) at $\Delta t = 0$ and specifies the ratio of the channel output power delivered by the magnetoionic component to the channel input power. Furthermore, the spectrums of $g_{sia}(t)$ and $\boldsymbol{g}_{sia}(t)$ are equal:

$$F\{E[g_{sia}(t)g_{sia}(t+\Delta t)]\} = F\{E[\boldsymbol{g}_{sia}(t)\boldsymbol{g}_{sia}(t+\Delta t)]\}. \tag{10}$$

Because $g_{sia}(t)$ and $\boldsymbol{g}_{sia}(t)$ are independent in (8), $G_{sia}(t)$ has a spectrum that is the sum of the identical spectrums of $g_{sia}(t)$ and $\boldsymbol{g}_{sia}(t)$ and it has even symmetry about $\nu = 0$. Therefore, $\exp\left(j2\pi\nu_{sia}t\right)$ was included with $G_{sia}(t)$ in (7) to provide the desired frequency shift ν_{sia} for this magnetoionic component. With the a subscript replaced by b, (8)–(10) also apply for the other magnetoionic component, the last term in (7).

The tap-gain correlation function corresponding to (7) is

$$C_{si}(\Delta t) = C_{sia}(0) \exp\left[-2\pi^2\sigma_{sia}^2(\Delta t)^2 + j2\pi\nu_{sia}\Delta t\right]$$
$$+ C_{sib}(0) \exp\left[-2\pi^2\sigma_{sib}^2(\Delta t)^2 + j2\pi\nu_{sib}\Delta t\right] \tag{11}$$

and the tap-gain spectrum is

$$v_{si}(\nu) = \frac{C_{sia}(0)}{(2\pi)^{1/2}\sigma_{sia}} \exp\left[-\frac{(\nu - \nu_{sia})^2}{2\sigma_{sia}^2}\right]$$
$$+ \frac{C_{sib}(0)}{(2\pi)^{1/2}\sigma_{sib}} \exp\left[-\frac{(\nu - \nu_{sib})^2}{2\sigma_{sib}^2}\right] \tag{12}$$

where

$$C_{si}(0) = C_{sia}(0) + C_{sib}(0). \tag{13}$$

Equation (12), of course, is illustrated by Fig. 2.

Since the stationary specific model we selected was a Gaussian-scattering model, the preceding specifications completely define it; no additional statistical descriptions are necessary. It can be seen that the model involves three assumptions: 1) the Gaussian-scattering hypothesis, that each tap-gain function is a complex-Gaussian process; 2) the independence hypothesis, that each tap-gain function is independent; and 3) the Gaussian-spectrum hypothesis, that each tap-gain spectrum in general is the sum of two Gaussian functions of frequency. The purpose of our propagation measurements and analyses was to test the validity of these three hypotheses and to determine the practical bandwidth limitations of the model for typical channels. Because the discrete paths in the model only approximate the resolvable ionospheric modal components with nonzero time spreads, the model, strictly speaking, can be valid only over an arbitrarily small bandwidth. Practically, however, as will be shown, it can be considered valid over a larger bandwidth B that is inversely proportional to the amount of time spreading on the resolvable ionospheric model components represented by each tap.

MEASUREMENTS

A hybrid time-and-frequency-domain method was used to obtain propagation measurements. In the transmitter, an accurate cesium-beam frequency standard was used to generate a carrier that was amplitude modulated to obtain coherent pulses with near-Gaussian envelopes of 50-μs duration at a 200-Hz rate. The same reference was used to generate 11 CW signals (tones) of equal amplitude at frequencies that coincided with 11 of the spectral components of the pulses. The spectrum of the composite signal is illustrated in Fig. 3. The 11 tones were symmetrically spaced in a 9.6-kHz band about the carrier frequency f_6 and were numbered $f_1, f_2, \cdots, f_k, \cdots, f_{11}$. The low-level composite signal was amplified linearly to a 5-kW peak power level and transmitted over a sloping V antenna with a
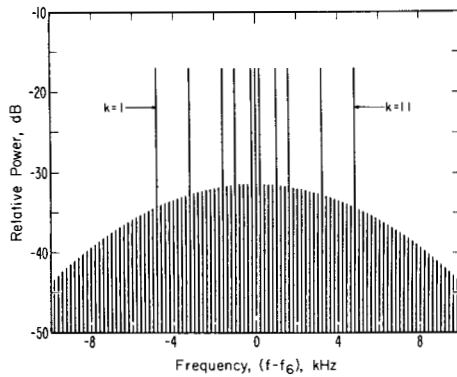
Fig. 3. Transmitter power spectrum.

broad vertical pattern that covered the takeoff angles of the expected ionospheric modes.

The signal was received over a sloping V antenna with the same broad vertical pattern. In the receiver, each of the 11 tones (with delays and modulation imposed by the ionospheric channel) was separated and heterodyned to a second IF of 80 Hz, using local oscillator signals derived from a rubidium frequency standard. The received signal was also passed through an 11-notch filter that removed the 11 tones, and the resulting pulses were envelope detected and compared against a 200-Hz reference derived from the rubidium standard to obtain measurements of $\{\tau_i\}$. The 80-Hz IF tones were FM recorded on an analog tape recorder with an 80-Hz reference signal (a composite of sine and cosine square waves) from the rubidium standard. During later playback, the reference signals were used to detect each of the 11 IF tones to obtain the real and imaginary components of the time-varying frequency responses of the measured channel $H_m(f_k,t)$ at the 11 values of f_k. The detection bandwidth was 8 Hz, an order of magnitude greater than needed. The 22 real baseband functions were sampled at either 3.125 or 6.25 Hz, converted to digital form, and tape recorded for computer analysis. The analog-to-digital (A–D) conversion of the data changed the set of complex functions that were continuous in time $H_m(f_k,t)$ to a corresponding set of sequences $H_m(f_k,t_r)$ with r an integer that consecutively numbers the equally spaced sampling times.

All portions of the measuring system (including the A–D conversion and computer programs) were thoroughly tested prior to the measurements. The measurement errors in the entire system (primarily wow and flutter from the analog recorder) were more than 30 dB below the rms level of $H_m(f_k,t_r)$.

Propagation measurements were made over a 1294-km link between Long Branch, Ill. (40°13′ N, 90°01′ W), and Boulder, Colo. (40°08′ N, 105°14′ W). Nighttime measurements were made on 5.864 MHz and daytime measurements on 9.259 MHz, both sufficiently below the predicted maximum usable frequency to make it probable that both one- and two-hop modes would be seen. While the system held calibration extremely well, the calibration was checked

about once an hour to ensure accurate measurements. About 7 hours of recorded nighttime measurements and 10 hours of daytime measurements were obtained during three periods in November, 1967. Continuous strip-film recordings of an oscilloscope intensity presentation of the received pulses were made and subsequently visually examined to select data for analysis. Avoiding times near sunrise and sunset, when propagation conditions were changing rapidly, samples were selected that appeared typical and reasonably stationary. Three of these samples of 10- to 13-minute duration from day and night measurements were analyzed. In the description of the results, these samples will be designated I1, I2, and I3.

ANALYSES

Deterministic Fit

The time-varying frequency response of the measured ionospheric channels can be described by

$$H_m(f_k,t_r) = \sum_{i=1}^{n} \exp\left(-j2\pi\tau_i f_k\right) G_{mi}(f_k,t_r) \qquad (14)$$

where each $G_{mi}(f_k,t_r)$ is a function of frequency because of the nonzero time spread on the ionospheric path about its mean time delay τ_i. But our model specified discrete paths with tap-gain functions $\{G_{si}(t)\}$ that were independent of frequency (i.e., the time-varying response of our model in (1) could match the ionospheric response in (14) only over an arbitrarily small band). To test the validity of our model, therefore, we wanted to obtain the response on each ionospheric mode at a single frequency, for example, $\{G_{mi}(f_6,t_r)\}$. While our measurements of $H_m(f_k,t_r)$ did not supply $\{G_{mi}(f_6,t_r)\}$ directly, approximations were obtained for each t_r by deterministically fitting the frequency response of the general model to that of the measured channel in a least-squares manner over a limited bandwidth B_d centered on the carrier frequency f_6. This was done by solving the set of $2l + 1$ linear equations

$$\sum_{i=1}^{n} \exp\left(-j2\pi\tau_i f_k\right) G_{di}(t_r) = H_m(f_k,t_r),$$

$$k = 6 - l, 7 - l, \cdots, 6 + l \qquad (15)$$

for $\{G_{di}(t_r)\}$, where the number of equations (values of k) used $n \le (2l + 1) \le 11$ determined the bandwidth B_d. The solutions for $\{G_{di}(t_r)\}$ were therefore approximations of $\{G_{mi}(f_6,t_r)\}$ and defined a deterministic channel with a response $H_d(f_k,t_r)$ that was a least-squares approximation of $H_m(f_k,t_r)$.

For the solutions $\{G_{di}(t_r)\}$ to be accurate approximations of $\{G_{mi}(f_6,t_r)\}$, it was necessary to observe two constraints: 1) the bandwidth B_d occupied by the $2l + 1$ tones used in (15) had to be much smaller than the reciprocal of the time spread on each ionospheric path, so that each $G_{mi}(f_k,t_r)$ would be nearly constant in frequency over B_d, and 2) B_d needed to be greater than about one

half of the reciprocal of the smallest of the differential propagation times of the paths to adequately resolve them. The frequency separations of adjacent tones in the transmitter spectrum were purposely made smaller near the carrier so that $2l + 1$ could exceed n while meeting the bandwidth constraints.

Because B_d could not ideally meet the bandwidth constraints in the deterministic fit, errors were introduced into each $G_{di}(t_r)$ that were inversely related to its strength. To explain the errors caused by B_d being too large, consider error-free measurements of a hypothetical ionospheric channel in which all paths are discrete except path one ($i = 1$). Because $G_{m1}(f_k, t_r)$ for path one is not constant in frequency over B_d, the least-squares fit of $H_d(f_k, t_r)$ to $H_m(f_k, t_r)$ will have an error

$$E_H(f_k, t_r) = H_d(f_k, t_r) - H_m(f_k, t_r) \qquad (16)$$

at all frequencies, and each $G_{di}(t_r)$ will have an error

$$E_{Gi}(t_r) = G_{di}(t_r) - G_{mi}(f_6, t_r). \qquad (17)$$

The magnitudes of the latter deterministic tap-gain function errors will be comparable, and each will be proportional to $| G_{mi}(f_6, t_r) |$ for path one (if $G_{mi}(f_6, t_r) = 0$, (16) and (17) will be zero). The error component in each $G_{di}(t_r)$ consequently will vary in time according to path one, and the error components in the various $G_{di}(t_r)$ will be highly correlated with each other and with the tap-gain function for path one. In an actual ionospheric channel, where all of the ionospheric modal components have nonzero time spreads, each $G_{di}(t_r)$ will have a number of error components, one from each of the other paths, whose magnitudes are proportional to the strengths and time spreads of the corresponding paths. As a result of this crosstalk, tap-gain function solutions for weak paths contain the largest fractional amount of undesired crosstalk from the other paths, with the strongest crosstalk coming from the strongest path.

In a similar way, errors of measurement will introduce errors into $\{G_{di}(t_r)\}$ that increase very rapidly when B_d becomes too small. Such errors in each $G_{di}(t_r)$ are highly correlated with the errors in the other solutions, and their fractional size is also inversely related to the strength of the path.

In our analyses of the three samples of data, we obtained a measure of the errors in the deterministic fit by computing $| \hat{E} |/| \hat{H}_m |$, where the hats indicate the rms values of the magnitudes over the tones in B_d and the sample duration.

Statistical Fit

For each mode in each sample, we computed the deterministic tap-gain correlation function

$$C_{di}(\Delta t) = \frac{1}{m_a'} \sum_{r=1}^{m_a'} G_{di}^*(t_r) G_{di}(t_r + \Delta t) \qquad (18)$$

where m_a' was the actual number of values m_a in the sample minus the number in Δt. To determine the optimum

values of $C_{sia}(0)$, $C_{sib}(0)$, ν_{sia}, ν_{sib}, σ_{sia}, and σ_{sib}, we first equated the path power ratios:

$$C_{si}(0) = C_{di}(0) \qquad (19)$$

and then fitted $C_{si}(\Delta t)$ to $C_{di}(\Delta t)$ by least squares; i.e., $| C_{si}(\Delta t) - C_{di}(\Delta t) |^2$ was minimized over the interval in Δt in which the values of $C_{di}(\Delta t)$ were large enough to be significant.

Hypotheses Tests

Successive values of $G_{di}(t_r)$ were highly correlated for each path, because the sampling rate was many times greater than the frequency spread (fade rate) on each path. It was therefore necessary to estimate the effective number of independent values in each $G_{di}(t_r)$, in order to test the Gaussian-scattering, independence, and Gaussian-spectrum hypotheses. For each path, the effective number of independent values was computed from

$$m_{ei} = 2B_{ei} t_m \qquad (20)$$

where B_{ei} is the statistical bandwidth [30] of the path and t_m is the duration of the sample. The six optimum parameters obtained for $C_{si}(\Delta t)$ in the statistical fit were used to compute the statistical bandwidth. The justification for this estimate will not be presented but is available [31].

To test the Gaussian-scattering hypothesis for each path in each sample, the linear phase component was removed from $G_{ci}(t_r)$, and amplitude and phase histograms were computed for the modified function. A chi-square test [30] was applied to each histogram to determine whether the observed amplitude distribution could be accepted as Rayleigh and the phase distribution as uniform. The computed chi-square values χ_i^2 were normalized by dividing them by the tabulated chi-square values χ_{Ti}^2 for a significance level of 0.1, and the appropriate number of degrees of freedom:

$$\overline{\chi_i^2} = \chi_i^2 / \chi_{Ti}^2 \qquad (21)$$

was computed, and $\overline{\chi_i^2} \le 1$ was used as a criterion of acceptance.

It can be argued that a function may have a Rayleigh amplitude distribution and a uniform phase distribution and yet not be complex-Gaussian, as defined by (7)–(10). While hypothetical functions of this type can be defined, the probability of such functions occurring in any natural physical process is extremely small. If a natural process exhibits a Rayleigh amplitude and a uniform phase distribution, it may be considered certain that the process is complex-Gaussian.

To test the independence hypothesis, the tap-gain functions $\{G_{di}(t_r)\}$ were cross correlated using

$$| \Gamma_{il} | = \left| \frac{1}{m_a} \sum_{r=1}^{m_a} \bar{G}_{di}^*(t_r) \bar{G}_{dl}(t_r) \right|,$$

$$i = 1, 2, \cdots, (n - 1),$$

$$l = (i + 1), (i + 2), \cdots, n \qquad (22)$$

where the bars above the tap-gain functions indicate they were normalized $[C_{di}(0) = C_{dl}(0) = 1]$. If the paths in the ionospheric channel were independent, the estimate from (22) would still be greater than zero because of the finite number of values in the sample. For independent complex-Gaussian tap-gain functions, it was shown [31] that $|\Gamma_{il}|$ would have very nearly a Rayleigh distribution, and that a conservative estimate of the rms value of this distribution would be

$$\epsilon_{il} = 1/(m_{eil})^{1/2} \qquad (23)$$

where m_{eil} is the larger of m_{ei} and m_{cl}, which are the effective numbers of independent values in paths i and l, respectively. For a valid hypothesis, $|\Gamma_{il}|$ would exceed $1.52\epsilon_{il}$ with a probability of 0.1; therefore,

$$|\bar{\Gamma}_{il}| = |\Gamma_{il}|/(1.5\epsilon_{il}) \qquad (24)$$

was computed, and $|\bar{\Gamma}_{il}| \leq 1$ was used as a criterion of acceptance that the tap-gain functions were uncorrelated and consequently independent if the Gaussian-scattering hypothesis had been shown to be valid.

To test the validity of the Gaussian-spectrum hypothesis for each path, a statistical test was performed on

$$|\Delta\bar{C}_i(\Delta t)| = |\bar{C}_{si}(\Delta t) - \bar{C}_{di}(\Delta t)|. \qquad (25)$$

Since a tap-gain spectrum is the Fourier transform of the corresponding tap-gain correlation function, $|\Delta\bar{C}_i(\Delta t)|$ was a measure of how well each tap-gain spectrum in the model fitted the corresponding spectrum in the ionospheric channel. However, even if the path spectrums in the ionospheric channel were each composed of either one or two truly Gaussian components, a nonzero difference in the spectrums, and consequently in $|\Delta\bar{C}_i(\Delta t)|$, would be expected because of the finite number of values in the sample. The distribution of $\Delta\bar{C}_i(\Delta t)$ for valid Gaussian-scattering and Gaussian-spectrum hypotheses was derived [31] and shown to be complex-Gaussian with unequal quadrature components. Its magnitude (25) varied from the right half of a zero-mean Gaussian distribution at $\Delta t = 0$ to a Rayleigh distribution as $C_{si}(\Delta t) \rightarrow 0$. For both of these limiting cases, the rms value was

$$\epsilon_{ci} = 1/(m_{ei})^{1/2}. \qquad (26)$$

While rms values at intermediate values of Δt were not known, they were assumed to be the same. For each path γ_i the rms value of $|\Delta\bar{C}_i(\Delta t)|$ over its significant interval was computed. Since $|\Delta\bar{C}_i(\Delta t)|$ would exceed $1.64\epsilon_{ci}$ for a half-Gaussian distribution and $1.52\epsilon_{ci}$ for a Rayleigh distribution with probabilities of 0.1,

$$\bar{\gamma}_i = \gamma_i/(1.5\epsilon_{ci}) \qquad (27)$$

was computed, and $\bar{\gamma}_i \leq 1$ was used as a criterion of acceptance for the Gaussian-spectrum hypothesis.

Bandwidth Limitations

Since the statistical tests that were made to confirm the validity of the three hypotheses, and thereby the validity of the channel model, were based on measurements made over a bandwidth B_d in which the individual ionospheric path responses $\{G_{mi}(f_k,t_r)\}$ were reasonably constant, confirmation of the model implied that it was valid over this bandwidth. However, the model can be considered valid over a larger bandwidth B without introducing excessive error. To determine the limitation on B imposed by the nonzero time spreads on the ionospheric paths, for each sample we computed the channel correlation function for the ionospheric channel along the Δf axis from

$$R_m(\Delta f,0) = \frac{1}{m_a}\sum_{r=1}^{m_a} H_m^*(f_k,t_r)H_m(f_k + \Delta f,t_r),$$

$$\Delta f = f_l - f_k, \qquad k = 1,2,\cdots,11,$$

$$l = k, k+1, \cdots, 11. \qquad (28)$$

The corresponding channel correlation function for the model $R_s(\Delta f,0)$ was computed from (13) and (5), using the values of $C_{sia}(0)$ and $C_{sib}(0)$ obtained in the statistical fit. The discrepancies in the two channel correlation functions were computed from

$$|\Delta\bar{R}(\Delta f,0)| = |\bar{R}_s(\Delta f,0) - \bar{R}_m(\Delta f,0)|. \qquad (29)$$

In each sample, the values in (29) fluctuated about a linear component that increased from zero as Δf increased from zero. The value of Δf at which the linear component became 0.2 was arbitrarily selected as a reasonable measure of the bandwidth B over which the model might be considered valid. To determine this bandwidth, a hypothetical ionospheric channel was assumed in which each path had the same time spreading with a Gaussian distribution of standard deviation ρ. For this channel, it was shown that the 0.2 correlation would occur when Δf was about one fourth of the reciprocal of the time spreads 2ρ. Therefore,

$$B = 1/[4(2\rho_e)] \qquad (30)$$

was used to determine $2\rho_e$ the effective time spreads on the ionospheric paths.

Channel Characteristics

As a matter of interest, several statistical descriptions of the fitted channel model were computed for each sample. The relative channel time delay τ_s is defined as the first moment of the normalized channel scatter function $s_s(\tau,\nu)/R_s(0,0)$ with respect to time:

$$\tau_s = \int_{-\infty}^{\infty} \tau \int_{-\infty}^{\infty} \frac{s_s(\tau,\nu)}{R_s(0,0)}\,d\nu\,d\tau \qquad (31)$$

and measures the weighted average of the path time delays relative to an arbitrary $\tau = 0$. The channel time spread $2\rho_s$ is defined as two times the square root of the second central moment of the normalized channel scatter function with respect to time:

$$2\rho_s = 2\left[\int_{-\infty}^{\infty} (\tau - \tau_s)^2 \int_{-\infty}^{\infty} \frac{s_s(\tau,\nu)}{R_s(0,0)}\,d\nu\,d\tau\right]^{1/2} \qquad (32)$$

and measures the effective time spread in the channel. The channel frequency shift ν_s and the channel frequency spread $2\sigma_s$ were computed in an analogous way with respect to frequency, except a true $\nu = 0$ reference was used.

RESULTS

Descriptions of the measurements, results of the analyses, and characteristics of the channel in each sample of data, I1, I2, and I3, are presented in Table I. The results of the analyses for the individual paths in each sample are presented in Table II. Each sample will be discussed in turn.

Sample I1

The first sample of data was obtained from daytime measurements when low rays of three modes were present (1E, 1F, and 2F) with the relative time delays listed in Table II. An examination of $\{C_{di}(\Delta t)\}$ showed that only the 1E mode exhibited a significant separation of the magnetoionic components in frequency. In the statistical fits of $C_{si}(\Delta t)$ to $C_{di}(\Delta t)$, therefore, two magnetoionic components were specified for path one in the channel model and single components for paths two and three. The resulting optimum parameters for each path in the channel model (power ratios, frequency shifts, and frequency spreads) are listed in Table II. It can be seen that each magnetoionic component in the 1E mode had a frequency spread on the order of 0.01 Hz, corresponding to a very slow fade rate. As a result, the effective number of independent values in the sample for path one was only 30, as listed in Table II. The frequency spreads on the 1F and 2F modes were about an order of magnitude larger, making the effective number of independent values for these paths correspondingly larger. Consequently, one would expect the error in the fit of $C_{si}(\Delta t)$ to $C_{di}(\Delta t)$ to be noticeably less for the second and third paths than for the first path, as was the case.

In the results of the chi-square tests of the Gaussian-scattering hypothesis that are listed in Table II for each path, the first value is for the Rayleigh amplitude distribution test, and the second is for the uniform phase distribution test. Since all normalized chi-square values for I1 were less than one, the Gaussian-scattering hypothesis was accepted as valid for this sample. The normalized tap-gain correlation function error $\bar{\gamma}_i$ was less than one for two paths and only slightly greater than one for the third path. Since the probability is fairly high (about 0.3) that one or more of the three values would exceed one for a valid Gaussian-spectrum hypothesis (assuming a valid independence hypothesis), the Gaussian-spectrum hypothesis was accepted as valid for Sample I1. Since $|\bar{\Gamma}_{il}|$, the normalized cross correlation between the ith and lth tap-gain functions, was less than one for all combinations, the independence hypothesis was also accepted as valid for I1.

To determine the bandwidth over which the channel model might be considered reasonably valid, we computed

TABLE I
SUMMARY OF CHANNEL DATA

	I1	I2	I3
Frequency, MHz	9.259	9.259	5.864
Date, 1967	November 30	November 30	November 10
Time, MST (GMT-07:00)	10:15–10:28	11:10–11:20	04:17–04:30
Sampling rate, Hz	3.125	6.250	3.125
Actual number of values m_a	2437	3750	2437
Tones used in deterministic fit k	3, 4, $\cdots$, 9	3, 4, $\cdots$, 9	3, 4, $\cdots$, 9
Bandwidth of deterministic fit B_d, kHz	3.2	3.2	3.2
Error in deterministic fit $\|\hat{E}\| / \|\hat{H}_m\|$, dB	-15.4	-15.5	-8.2
Bandwidth of model B, kHz	12	8	2.5
Effective path time spreads $2\rho_e$, µs	20	30	100
Relative channel time delay τ_s, µs	137	173	589
Channel time spread $2\rho_s$, µs	478	520	464
Channel frequency shift ν_s, Hz	0.0013	0.0171	0.110
Channel frequency spread $2\sigma_s$, Hz	0.123	0.140	0.0666

$|\Delta\bar{R}(\Delta f, 0)|$ from (29). The linear component had a value of 0.2 at $\Delta f = B = 12$ kHz, with a corresponding effective path time spread $2\rho_e = 20$ µs. These values with other computed channel characteristics are listed in Table I.

Sample I2

The second sample of data was taken about 1 hour later than I1 and differs primarily in the presence of a weak M mode that was not present in I1. (An M mode is a downward reflection from the F layer, an upward reflection from the E layer, and a second downward reflection from the F layer.) Again, only the 1E mode showed a frequency separation of the magnetoionic components, necessitating two components in the channel model. To illustrate the errors in the fits of $C_{si}(\Delta t)$ to $C_{di}(\Delta t)$, these functions (normalized) are presented in Figs. 4–7 for the four paths. (For the 1E, 1F, and 2F modes, the plots are similar to the corresponding functions in I1.) The form or shape of the error functions in Figs. 4–7 have no significance, of course, since their magnitudes are comparable to or less than $1/(m_{ei})^{1/2}$. The tap-gain spectrums $\{v_{si}(\nu)\}$ corresponding to the tap-gain correlation functions $\{C_{si}(\Delta t)\}$ are illustrated in Fig. 8, where the Gaussian functions appear as parabolas because of the logarithmic ordinate.

It is interesting to note the agreement between the frequency shifts and frequency spreads of the M and 2F modes in Table II and the corresponding agreements between the tap-gain correlation functions and tap-gain spectrums. This might be expected because the two F-layer reflection points on the M mode geographically were relatively close to those of the 2F mode, and the addi-

TABLE II
SUMMARY OF PATH DATA

Sample Number	Path Number, i	Mode	Relative Time Delay, τ_i (μs)	Relative Power Ratio, $\dfrac{C_{si}(0)}{R_s(0,0)}$ (dB)	Frequency Shift, ν_{sia}, ν_{sib}, ν_{si} (Hz)	Frequency Spread, $2\sigma_{sia}$, $2\sigma_{sib}$, $2\sigma_{si}$ (Hz)	Effective Number Values, m_{ei}	Normalized Chi-Square Values, $\bar\chi_{i1}{}^2$, $\bar\chi_{i2}{}^2$	Normalized Auto-correlation Error, $\bar\gamma_i$	Path Pair, i,l	Normalized Cross Correlation, $|\bar\Gamma_{il}|$
I1	1a		40	−4.1	0.0022	0.0073				1,2	0.65
	1b		40	−4.3	0.0170	0.0318				1,3	0.59
	1	1E	40	−1.2	0.0094	0.0272	30.3	0.04, 0.47	0.25	2,3	0.68
	2	1F	290	−7.2	0.0089	0.144	198.5	0.24, 0.25	0.89		
	3	2F	1139	−13.5	−0.167	0.340	469.4	0.14, 0.26	1.06		
I2	1a		40	−4.1	−0.0008	0.0064				1,2	1.11
	1b		40	−5.5	0.0127	0.0084				1,3	3.74
	1	1E	40	−1.7	0.0071	0.0153	15.0	0.06, 0.03	0.34	1,4	2.88
	2	1F	290	−5.9	0.0159	0.180	191.4	0.12, 0.23	0.65	2,3	0.83
	3	M	590	−17.6	0.108	0.334	354.7	0.48, 0.16	1.22	2,4	1.62
	4	2F	1126	−12.6	0.118	0.336	356.8	0.42, 0.18	0.84	3,4	5.59
I3	1a		445	−3.8	0.0764	0.0360				1,2	0.95
	1b		445	−5.7	0.134	0.0320				1,3	0.97
	1	unknown	445	−1.6	0.0989	0.0658	88.3	0.39, 0.08	0.23	2,3	1.39
	2a		750	−10.8	0.121	0.0104					
	2b		750	−10.6	0.141	0.0130					
	2	unknown	750	−7.7	0.131	0.0229	30.5	0.47, 0.08	0.15		
	3a		1088	−12.9	0.121	0.0149					
	3b		1088	−10.4	0.151	0.0206					
	3	unknown	1088	−8.5	0.140	0.0335	45.4	0.68, 0.11	0.66		

tional frequency shift and frequency spread imposed on the M mode by its upward reflection from the E layer were relatively small.

Since the normalized chi-square values for I2, as listed in Table II, were all less than one, the Gaussian-scattering hypothesis was accepted as valid for I2. Since three of the four normalized tap-gain correlation errors $\{\bar\gamma_i\}$ were less than one, and the probability that one or more would be greater than one for a valid Gaussian-spectrum hypothesis was about 0.34 (assuming independence), the Gaussian-spectrum hypothesis was accepted as valid for I2.
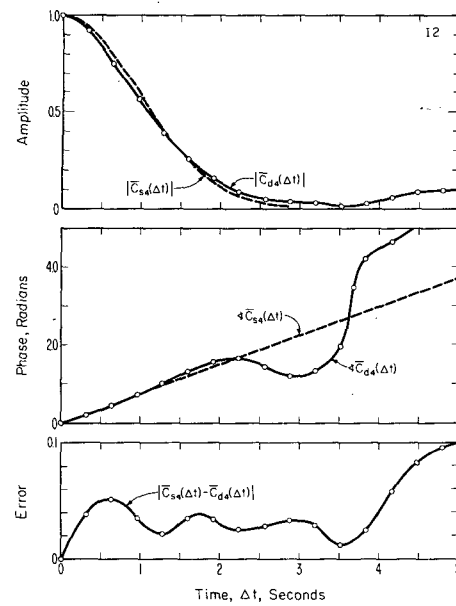
Four of the normalized cross correlations between the tap-gain functions were considerably greater than one (pairs 1,3; 1,4; 2,4; and 3,4), which indicates these pairs of modes were significantly correlated. However, it seems likely that these indications are false and that the numbers are excessively high because of crosstalk. It is known that crosstalk will cause the highest erroneous cross correlations both between a strong mode and a weak mode and between two weak modes. Since the large cross correlation values follow this pattern, we decided that the cross correlation results could not be trusted, and that the independence hypothesis test was inconclusive. The probable reason the crosstalk was large in I2 and not in I1, which had an equal value of B_d, was because of the 50 percent greater effective path time spreads $2\rho_e$, as well as the presence of the very weak M mode in I2. A somewhat smaller value of B_d should have been used in I2. It is unfortunate that the test was inconclusive in I2 since the M and $2F$ modes might not be expected to be independent because of the relative closeness of their F-layer reflection points.

Plots of $\bar R_m(\Delta f,0)$ and $\bar R_s(\Delta f,0)$ and the magnitude of their difference are presented in Fig. 9. The major oscillation in the magnitude and phase plots is caused, of course, by the two strongest modes, with the 4-kHz period being equal to the reciprocal of the 250-μs differential delay time. Weaker oscillations are caused by the other path combinations. It can be seen that the linear component of the error curve has a value of 0.2 at $\Delta f = B = 8$ kHz, corresponding to an effective path time spread $2\rho_e = 30$ μs.

Sample I3

The third sample of data was obtained from nighttime measurements when three paths were present whose identity is not certain. Since $\{C_{di}(\Delta t)\}$ clearly showed that the magnetoionic components were significantly separated in frequency on all three modes, two components were used for each of the three paths in the statistical fits. The resulting optimum power ratios, frequency shifts, and frequency spreads are listed in Table II. The tap-gain correlation functions for path $i = 1$ are illustrated in Fig. 10. The tap-gain spectrums for the channel model for all three paths are presented in Fig. 11 and show that the power ratios and frequency spreads for the two magnetoionic components in each path are approximately equal.

Since the normalized chi-square values for I3 in Table II were all less than one, the Gaussian-scattering hypothesis was accepted as valid. The normalized tap-gain correlation errors $\{\bar\gamma_i\}$ obtained from the statistical fit also were all less than one, so the Gaussian-spectrum hypothesis was accepted as valid for Sample I3. One of the
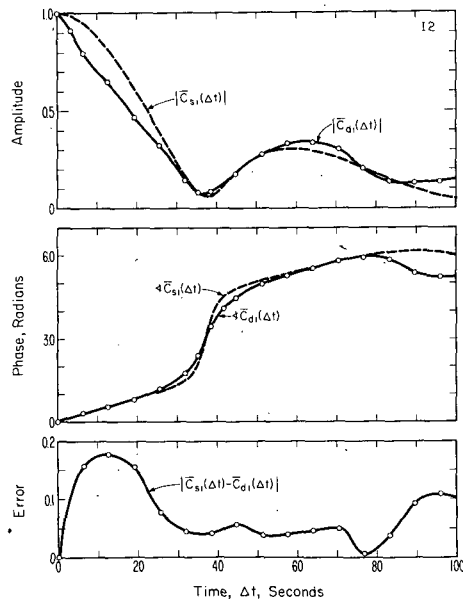
Fig. 4.   Tap-gain correlation functions for path $i = 1$ in Sample I2.
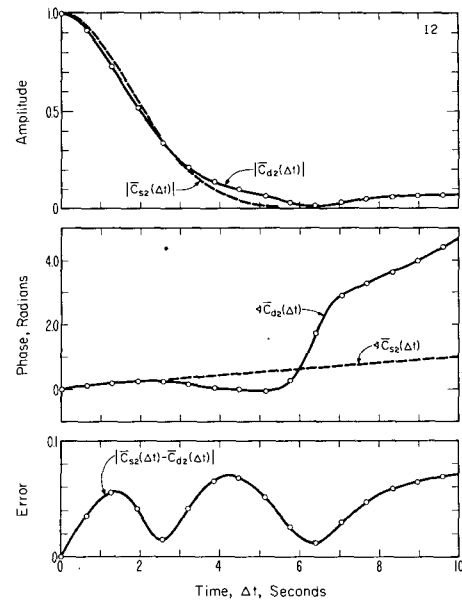
Fig. 6.   Tap-gain correlation functions for path $i = 3$ in Sample I2.
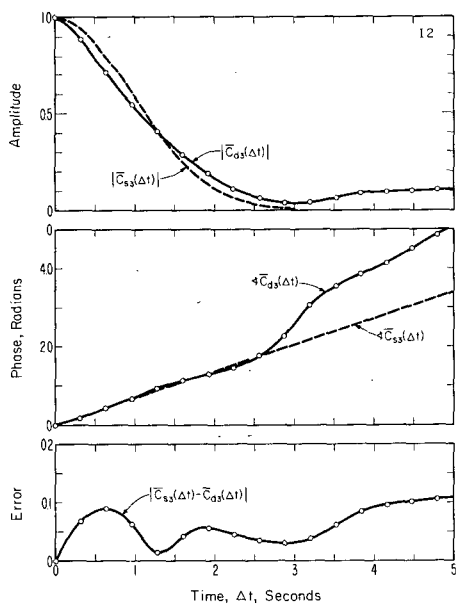
Fig. 5.   Tap-gain correlation functions for path $i = 2$ in Sample I2.

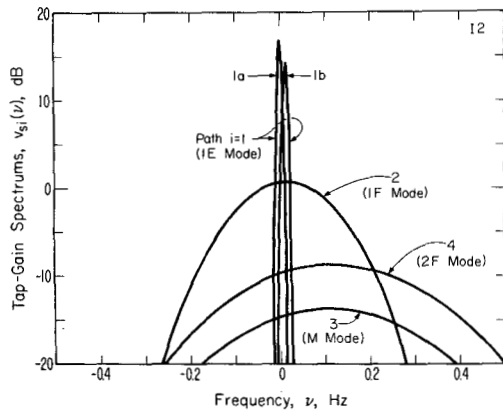Fig. 7.   Tap-gain correlation functions for path $i = 4$ in Sample I2.

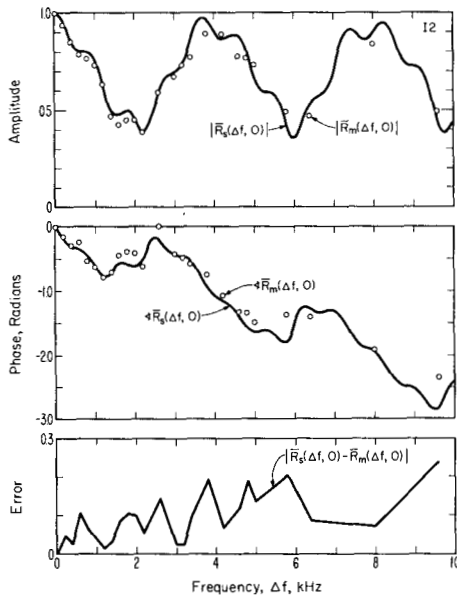Fig. 8. Tap-gain spectrums for channel model in Sample I2.

Fig. 9. Channel correlation functions along frequency axis for Sample I2.

Fig. 10. Tap-gain correlation functions for path $i = 1$ in Sample I3.

Fig. 11. Tap-gain spectrums for channel model in Sample I3.

three normalized cross correlations $|\bar{\Gamma}_{23}|$ between the two weakest paths was somewhat greater than one. However, the relatively large error in the deterministic fit ($|\hat{E}|/|\hat{H}_m| = -8.2$ dB) indicated that the crosstalk for this sample was sufficiently large to cause an erroneously high cross correlation for paths two and three despite their fairly large relative power ratios. For this reason, and because for a valid independence hypothesis in the absence of crosstalk, the probability that one or more normalized cross correlations would be greater than one was fairly high (0.3), we concluded that the independence hypothesis was valid.

The linear component in $|\Delta\bar{R}(\Delta f,0)|$ was found to have a value of 0.2 at $\Delta f = B = 2.5$ kHz, with a resulting effective path time spread of 100 μs. These and other computed channel characteristics for I3 are listed in Table I.

To make certain that the relatively large rms error in the deterministic fit in I3 was caused by the relatively large effective path time spreads of 100 μs, we partially
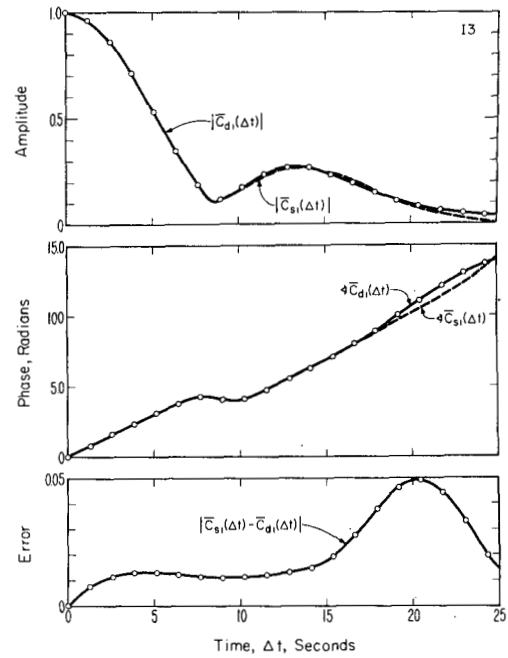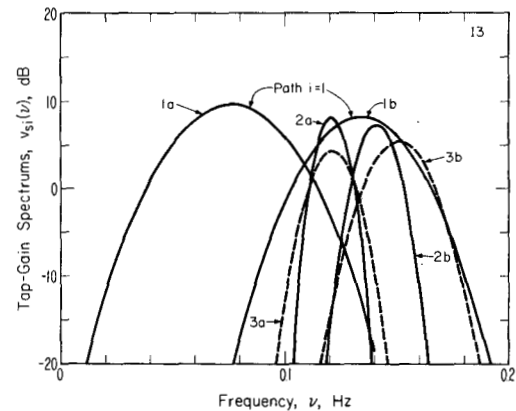
reanalyzed the I3 measurements, using a smaller value of $B_d = 2.0$ kHz. The resulting rms error in the deterministic fit was $|\hat{E}|/|\hat{H}_m| = -24.1$ dB. This probably was a more nearly optimum choice for B_d because of the large effective path time spreads, but a time limitation prevented the completion of the analyses with this smaller value of B_d. In all of the analyses our fear was that we would select a value of B_d that was too small: while the computation of the rms error in the deterministic fit was a good indication of excessive crosstalk because B_d was too large for the effective path time spreads in the channel, we had no corresponding test to determine whether excessive crosstalk was likely because B_d was too small.

CONCLUSIONS

Based on the measurements and analyses, we concluded.

1) Within the inherent limitations of the measuring and analysis techniques, it was shown for the measured ionospheric channels that the Gaussian-scattering, inde-

pendence, and Gaussian-spectrum hypotheses were valid, thereby making the proposed stationary channel model valid.

2) Based on the effective number of independent values, the reliability of the conclusions of validity for the Gaussian-scattering and Gaussian-spectrum hypotheses was greatest for the daytime F-layer modes $(1F, 2F,$ and $M)$, and least for the daytime E-layer mode $(1E)$.

3) For practical applications, the channel model can be considered valid over a bandwidth that is approximately one fourth of the reciprocal of the effective time spreads on the ionospheric paths. For the measured channels, these bandwidths were 2.5 kHz for the nighttime sample to a maximum of 12 kHz for the daytime samples. If the time spreading on each measured nighttime path was caused primarily by the differential propagation time between the two magnetoionic components, the model would be valid over a larger bandwidth if separate taps were used for each magnetoionic component.

4) In the measured channels, the frequency spreads on the two magnetoionic components of the low ray in the daytime F-layer modes were approximately equal and large compared to their differential frequency shifts, making only a single Gaussian function necessary in the tap-gain spectrums in the model. On the daytime E-layer-only modes and all of the nighttime modes, the frequency spreads on the magnetoionic component pairs were comparable to the differential frequency shifts, making two Gaussian functions necessary in the tap-gain spectrums in the model.

5) When two Gaussian components were required in a tap-gain spectrum, their power ratios were comparable, and their frequency spreads were approximately equal. This suggests that the model might be simplified by equating the power ratios and the frequency spreads of the two magnetoionic components.

6) Since other measurements and analyses have shown HF modal components usually exhibit Rayleigh fading, and since components with time spreads comparable to the measured paths are common, it appears reasonable to assume that the stationary channel model is valid for practical bandwidths for a large percentage, if not a majority, of typical HF ionospheric channels.

7) Additional measurements and analyses are desirable for other frequencies and links of different lengths and geographical locations to determine the conditions under which the model remains valid and the conditions under which modified or alternate models are necessary.

ACKNOWLEDGMENT

REFERENCES

[1] G. L. Turin, "Some computations of error rates for selectively fading multipath channels," *Proc. Nat. Electron. Conf.*, vol. 15, pp. 431–440, October 1959.
[2] P. A. Bello and B. D. Nelin, "The influence of fading spectrum on the binary error probabilities of incoherent and differentially-coherent matched filter receivers," *IRE Trans. Commun. Syst.*, vol. CS-10, pp. 160–168, June 1962.
[3] ——, "The effect of frequency selective fading on the binary error probabilities of incoherent and differentially coherent match filter receivers," *IEEE Trans. Commun. Syst.*, vol. CS-11, pp. 170–186, June 1963.
[4] R. F. Daly, "Analysis of multipath effects on FSK error probability for a simple HF channel model," Stanford Research Institute, Menlo Park, Calif., Res. Memo. 1, Contract SD-189, pp. 1–19, February 1964.
[5] P. A. Bello and B. D. Nelin, "Optimization of subchannel data rate in FDM-SSB transmission over selectively fading media," *IEEE Trans. Commun. Syst.*, vol. CS-12, pp. 46–53, March 1964.
[6] P. A. Bello, "Selective fading limitations of the Kathryn modem and some system design considerations," *IEEE Trans. Commun. Technol.*, vol. COM-13, pp. 320–333, September 1965.
[7] ——, "Binary error probabilities over selectively fading channels containing specular components," *IEEE Trans. Commun. Technol.*, vol. COM-14, pp. 400–406, August 1966.
[8] R. F. Daly, "Dispersion-limited error probabilities for correlated FSK diversity receptions," Stanford Research Institute, Menlo Park, Calif., Res. Memo. 1, Contract DCA-100-66-C-0075, pp. 1–25, March 1967.
[9] W. J. Bray, H. G. Lillicrap, and F. C. Owen, "The fading machine and its use for the investigation of the effects of frequency-selective fading," *J. Inst. Elec. Eng.*, vol. 94, pt. IIIA, pp. 283–297, 1947.
[10] A. H. Ross and H. F. Meyer, "Design and application of a multipath simulator," Signal Corps Engineering Laboratories, Fort Monmouth, N. J., Eng. Rep. E-1025, pp. 1–19, June 1948.
[11] H. B. Law, F. J. Lee, R. C. Looser, and F. A. W. Levett, "An improved fading machine," *Proc. Inst. Elec. Eng.*, vol. 104, pt. B, pp. 117–147, March 1957.
[12] M. J. DiToro, J. Hanulec, P. Ahrens, and M. Glass, "HF antimultipath device (adapticom)," U. S. Army Electronics Research and Development Laboratories, Fort Monmouth, N. J., Final Rep., Contract DA-36-039-AMC-02339(E), pp. 4-9–4-12, June 1964.
[13] R. Freudberg, "Laboratory simulator for frequency selective fading," *1965 IEEE Communications Conv. Rec.*, pp. 609–614, June 1965.
[14] W. F. Walker, "A simple baseband fading multipath channel simulator," *1965 IEEE Communications Conv. Rec.*, pp. 615–617; also *Radio Sci.*, vol. 1, pp. 763–767, July 1966.
[15] B. Goldberg, R. L. Heyd, and D. Pochmerski, "Stored ionosphere," *1965 IEEE Communications Conv. Rec.*, pp. 619–622.
[16] K. K. Clarke, "Random channel simulation and instrumentation," *1965 IEEE Communications Conv. Rec.*, pp. 623–629.
[17] E. W. Chapin and W. K. Roberts, "A radio propagation and fading simulator using radio-frequency acoustic waves in a liquid," *Proc. IEEE* (Letters), vol. 54, p. 1072, August 1966.
[18] M. S. Zimmerman and J. H. Horwitz, "A flexible transmission channel simulator," *1967 IEEE Int. Conf. on Communications Digest*, p. 73.
[19] M. S. Klein, "Synthetic HF environment," Rome Air Development Center, Rome, N. Y., Final Rep., Contract F20602-67-G0162, pp. 1–27, July 1968.
[20] R. J. Packer and J. A. S. Fox, "A simulator of ionospheric propagation of amplitude modulated signals," British Broadcasting Corp., Kingswood Warren, Tadworth, Surrey, U.K., Res. Dept. Rep. 1969/24, pp. 1–8, August 1969.
[21] C. C. Watterson, G. G. Ax, L. J. Demmer, and C. H. Johnson, "An ionospheric channel simulator," unpublished ESSA Tech. Memo ERLTM-ITS 198, pp. 1–44, September 1969.
[22] T. Hagfors, "Some properties of radio waves reflected from the moon and their relation to the lunar surface," *J. Geophys. Res.*, vol. 66, pp. 777–785, March 1961.
[23] P. A. Bello, "Characterization of randomly time-variant linear channels," *IEEE Trans. Commun. Syst.*, vol. CS-11, pp. 360–393, December 1963.
[24] R. G. Gallager, "Characterization and measurement of time- and frequency-spread channels," M.I.T. Lincoln Laboratory, Lexington, Mass., Tech. Rep. 352, pp. 1–34, April 1964.
[25] H. N. Shaver, B. C. Tupper, and J. B. Lomax, "Evaluation of a Gaussian HF channel model," *IEEE Trans. Commun. Technol.*, vol. COM-15, pp. 79–88, February 1967.

[26] M. Balser and W. B. Smith, "Some statistical properties of pulsed oblique HF ionospheric transmissions," *Radio Sci.*, vol. 66D, pp. 721–730, November/December 1962.

[27] J. T. Boys, "Statistical variations in the apparent specular component of ionospherically reflected radio waves," *Radio Sci.*, vol. 3, pp. 984–990, October 1968.

[28] K. Davies, "The measurement of ionospheric drifts by means of a Doppler shift technique," *J. Geophys. Res.*, vol. 67, pp. 4909–4913, November 1962.

[29] R. A. Shepherd and J. B. Lomax, "Frequency spread in ionospheric radio propagation," *IEEE Trans. Commun. Technol.*, vol. COM-15, pp. 268–275, April 1967.

[30] J. S. Bendat and A. G. Piersol, *Measurement and Analysis of Random Data.* New York: Wiley, 1966, pp. 146–150, 192–195, 264–267.

[31] C. C. Watterson, J. R. Juroshek, and W. D. Bensema, "Experimental verification of an ionospheric channel model," ESSA, Boulder, Colo., Tech. Rep. ERL 112-ITS 80, pp. 1–159, July 1969.

John R. Juroshek was born in Sheridan, Wyo., on January 7, 1940. He received the B.S. and M.S. degrees in electrical engineering from the University of Wyoming, Laramie, in 1961 and 1962, respectively. In 1966 he received a U. S. Department of Commerce training assignment for postgraduate study in communication theory at the University of California, Berkeley.

He was employed from 1962 to 1963 as an Electronic Engineer for the Federal Aviation Agency. In 1963 he joined the staff of the Central Radio Propagation Laboratory, Boulder, Colo., now the Institute for Telecommunication Sciences of the Office of Telecommunications. Since that time he has been associated with various research projects in communication technology. His present interests are in digital communications and channel characterization.

Mr. Juroshek is a member of Sigma Tau and Phi Beta Kappa.

Clark C. Watterson was born in Salt Lake City, Utah, on August 10, 1921. He received the B.S.E.E. degree with high honors from the University of Utah, Salt Lake City, in 1949. He has done graduate work at the University of Maryland, College Park, and the University of Colorado, Boulder.

From 1942 to 1960 he worked at the U.S. Naval Research Laboratory, Washington, D.C., on navigational aids and high-resolution radar. He was a guest worker at the Services Electronic Research Laboratory, England, during 1951–1952 doing work on pulsed microwave gas attenuators. Since 1960 he has been with the Department of Commerce, Boulder, Colo., doing work on information transmission, channel modeling, and channel simulation.

Mr. Watterson is a member of Tau Beta Pi and Phi Eta Sigma and is a Registered Professional Engineer in the State of Colorado.

William D. Bensema (S'58–M'58) was born in Chicago, Ill., on January 23, 1934. He received the B.S.E.E. degree from the University of Arizona, Tempe, in 1958.

He was employed by Philco Corporation for two years prior to joining the National Bureau of Standards, Boulder, Colo., in 1960, where he worked with an experimental multifrequency-shift teletype system. In 1965 he transferred to the Environmental Science Services Administration, Boulder, and worked in the area of atmospheric radio noise and atmospheric noise simulation. He is presently engaged in digital circuit design work for the Office of Telecommunications.